Heterogeneous photocatalytic degradation of metronidazole from aqueous solutions using Fe_3O_4/TiO_2 supported on biochar

Fatemeh Asgharzadeh[a], Mitra Gholami[b,c], Ahmad Jonidi Jafari[b,c], Majid Kermani[b,c], Hosseinali Asgharnia[d], Roshanak Rezaei Kalantary[b,c,]*

[a]_Environmental Health Engineering, School of Public Health, International Campus, Iran University of Medical Sciences, Tehran, Iran, email: asgharzadeh.59@gmail.com_
[b]_Department of Environmental Health Engineering, School of Public Health, Iran University of Medical Sciences, Tehran, Iran, Tel. +98 9123234586; email: rezaei.r@iums.ac.ir (R.R. Kalantary)_
[c]_Research Center for Environmental Health Technology, Iran University of Medical Sciences, Iran_
[d]_Department of Environmental Health Engineering, School of Public Health, Babol University of Medical Sciences, Babol, Iran_

ABSTRACT

The Fe_3O_4/TiO_2/BC composite was used as a photocatalyst to remove metronidazole from aqueous environments. The effect of different parameters such as pH, contact time, composite dose and initial metronidazole concentrations on the removal efficiency was investigated. Composite specifications were detected by field emission scanning electron microscopy, energy dispersive X-ray, X-ray diffraction, Fourier transform infrared spectroscopy, Brunauer–Emmett–Teller and vibrating sample magnetometer analyses. pH = 7 was selected as the optimal value with respect to composite pH_{zpc} and pK_a values of the metronidazole. The metronidazole removal efficiency increased with increasing composite concentrations (0.25–0.35 g L^{-1}). Also, the maximum efficacy was obtained at composite concentration of 0.35 g L^{-1}. With increasing initial antibiotic concentration (10–40 mg L^{-1}), the efficacy decreased from 100% to 80%. The kinetic data suggest that the photocatalytic removal of metronidazole followed the first-order kinetic model. A removal efficiency of 80% was maintained after five steps of composite application. The main mechanism involved in the photocatalytic removal of metronidazole is holes (h^+), hydroxyl radicals ($OH^\bullet$), and superoxide radicals ($O_2^{-\bullet}$).

Keywords: Fe_3O_4/TiO_2/BC composite; Metronidazole; Photocatalyst degradation

1. Introduction

The protection of the environment is undoubtedly one of the biggest issues facing humanity in the current century [1,2]. Emerging contaminants, as a large part of chemical compounds, include pharmaceutical compounds and personal care products, steroid hormones, industrial chemicals and herbicides [3–6]. Although these compounds are present in the aquatic environment at very low concentrations [7], most of the emerging contaminants are potentially carcinogenic and mutagenic [8,9]. Such pollutants can enter the environment from various sources such as municipal wastewater, pharmaceutical industries, landfills and industrial sewages [10]. Among these sources, the wastewater that is produced by urban wastewater treatment plants is considered as the main source [11,12]. Among emerging contaminants, pharmaceuticals and personal care products have created serious concern in environmental science communities and law enforcement agencies [13]. The inadequate removal of pharmaceuticals by conventional processes, and

* Corresponding author.

lack of legal guidelines and standards have caused many challenges in recent years [14,15]. The excessive use of such compounds has led to their widespread presence in the environment [16,17]. Approximately 95% of pharmaceuticals are excreted from the body, thereby being discharged in to the environment [18]. The annual consumption of antibiotics is estimated to be around 100,000–200,000 tons worldwide [19,20]. They are also used as food supplements and animal growth promoters in husbandries [21,22]. These compounds account for about 15% of all drugs used across the world [16]. They impose the highest toxic impact on microorganisms in the environment and, in turn, disturb the ecological balance [23,24]. These materials are classified according to their chemical structure or the mechanism of action [25]. The pharmaceutical industry wastewater contains the highest antibiotic concentration (20–800 mg L^{-1}) [26,27]. These substances also lead to an increase in the population of the resistant bacteria over other bacteria in the aeration tanks of urban wastewater treatment plants [11,12]. The nitrification, which is an important wastewater treatment process, can be impacted by the presence of a group of antibiotics and the growth of the nitrifying can be inhibited [28,29]. Algae are most sensitive to various antibiotics and form the basis of the food chain; thus, any reduction in the population of them may affect the balance of the aquatic system [30,31]. Metronidazole is one of the most widely used antibiotics around the globe. It belongs to the nitro imidazole group and imposes several effects on humans. Since this antibiotic cause lymphocyte DNA damage, it can be considered as a carcinogenic and mutagenic material. Of course, according to the International Agency for Research on Cancer (IARC), the mutagenesis of metronidazole, its genotoxicity for human cells and its carcinogen effect on humans have not yet been proved. Considering its low degradability and high solubility in water, this antibiotic is not removed from the water by conventional methods [32,33]. Its physical and chemical characteristics are summarized in Table 1.

The application of conventional processes for the treatment of antibiotic-laden wastewaters is restricted because physical methods usually produce secondary contaminants and biological methods are very time-consuming and less-efficient [34]. Advanced oxidation is a process, based on hydroxyl radical production, with a high oxidation capacity for degradation of contaminants such as toxins and pharmaceuticals, especially antibiotics that are resistant to degradation. Heterogeneous photocatalysts have been developed as an effective technology for wastewater decontamination [35,36]. Among these photocatalysts, TiO_2 has attracted special attention due to its high photo activity, non-toxic nature, high stability, and an extensive energy gap in higher electron production efficiency [37,38]. The TiO_2 photocatalytic activity is highly dependent on their microscopic structure and physical properties. Another way to increase the photocatalytic activity of TiO_2 is to prepare it based on a nano structure resulting in an increase in its surface area, which is directly related to its photocatalytic activity [38,39]. The application of TiO_2 powder in the form of a suspension is accompanied with problems such as the washing and dissolution of the catalyst and the filtration-based separation of the final catalyst during the treatment [40]. Therefore, the issue of catalytic stabilization has attracted a lot of attention. Many studies have been carried out to stabilize titanium on different substrates [38,41]. It should be noted that these approaches have been proposed as a solution for a solid-liquid separation; the slurry type reactor has significant advantages over those with stabilized catalyst due to having some characteristics like available surface area and mass transfer [38]. In a study on the photocatalytic activity of TiO_2/C, it was found that there is a synergistic impact and a common relationship between active carbon and TiO_2 in terms of their photocatalytic effect [38]. Several researchers have used various advanced oxidation processes for the metronidazole removal from aqueous solutions [33,38]. In the present study, a photocatalytic composite, with high photocatalytic activity and synergistic and combined effects, was prepared using the following three ways: (1) use of good catalytic potential of TiO_2; (2) use of biochar, as an adsorbent, with an optimal absorbance potential as a substrate; (3) use of the Fe_3O_4 nanoparticle for easy composite separation as well as the enhancement of photocatalytic potential. The magnetized $TiO_2/Fe_3O_4/BC$ composites showed a rapid accumulation under the influence of a magnetic field, which could be useful for separating these particles in further applications.

2. Materials and methods

All laboratory materials used in this study were of high purity grade. Chloride Iron(III) and chloride Iron(II), tetraethyl silicate, tetraethyl butyl titanium, ammonia, ethanol, methanol, acetonitrile were purchased from Merck Co. Inc., (Germany).

2.1. Substrate preparation

First, rice husks were collected from agricultural lands in the North of Iran. Next, they were washed well and rinsed using distilled water to remove any dust and impurities. They were then washed with acid to remove organic contamination and rinsed again with distilled water to obtain a neutral pH. Next, they were boiled to remove their color. Afterwards, they were dried by placing in an oven. Finally, they were calcinated inside a furnace under nitrogen gas at 700°C at a temperature rate of 5°C min^{-1} for 2 h [42].
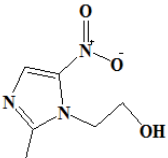
2.2. TiO_2 preparation

The TiO_2 nanoparticle was prepared using the sol–gel method. Hence, 0.1 M of tetraethyl butyl titanium was dissolved in 100 ml of ethanol and then placed on a stirrer for 10 min until a white precipitate was formed. Next, condensed HNO_3 was added to it in a drop-to-drop manner until the white color disappeared and a clear solution was obtained. The solution pH was adjusted at 4. A yellow precipitate was obtained after 6 h of stirring at room temperature. This process was continued for 10 h at 70°C to dry the precipitate and then a homogeneous substance was obtained. Finally, in order to calcinate the sample, it was placed in a tube furnace under nitrogen gas at 450°C for 2 h [43].

2.3. Preparation of magnetic biochar

The biochar surface was magnetized and saturated using the co-precipitation of Fe^{2+} and Fe^{3+} in an alkaline solution. An exact amount of ferrous chloride ($FeCl_2$) and

Table 1
Physicochemical characteristics and structure of metronidazole

Molecular formula: $C_6H_9N_3O_3$
Molar mass: 171.2 g mol^{-1}
$pk_a = 2.55$
Solubility: 9.5 g L^{-1}

ferric chloride ($FeCl_3$) with a weight ratio of 1–2.7, respectively, was poured in distilled water, which had been aerated with nitrogen gas for 30 min. Then, it was placed on a stirrer in the presence of nitrogen gas to be thoroughly mixed and dissolved. At this stage, the pre-prepared biochar was added before the addition of ammonia. After 30 min, 30 ml of ammonia was added; this led to the formation of a completely black precipitate. It was then completely stirred on a mantel for 60 min. Finally, when the precipitate achieved magnetic properties, it was separated by a high-strength magnet. It was then washed with distilled water and ethanol for several times, completely dried in an oven, and finally kept in a desiccator until the next use [43].

2.4. Preparation of $Fe_3O_4/TiO_2/BC$ composite

The TiO_2 prepared in the first stage was poured in 200 ml of distilled water and then placed on the stirrer for 30 min at room temperature. Afterwards, 2 g of the magnetized biochar was added to it and then placed on the stirrer for 30 min. It was later placed in an ultrasonic bath for 30 min to become completely homogeneous and thoroughly mixed on the stirrer for 45 min. It was finally separated by the magnet and washed with water and ethanol for several minutes. It was then completely dried in an oven and calcined in a cylindrical tube furnace at 450°C for 2 h. The magnetic biochar-TiO_2 ratio was adjusted at 1:2 [35,43,44].

2.5. Specifications of $Fe_3O_4/TiO_2/BC$ composite

The morphology, crystalline structure, surface area, functional group, and composite elements of the composite were identified by various analyses and devices. The X-ray diffraction (XRD) analysis was performed at room temperature to determine the crystal structure with a copper X-ray tube X wavelength of 1.44056 angstrom (Å), voltage of 40 kV, and current of 30 mA (Philips, Holland). The functional groups of the composite and substrate surfaces were identified by Fourier transform infrared spectroscopy (FTIR) (Thermo-AVATAR, American) in the range of 450–4,000 cm^{-1}. The surface morphology of the biochar composite was analyzed by scanning electron microscope (SEM) (TESCAN MIRA 3, Czech Republic). Also, the energy dispersive X-ray (EDX) analysis was used to identify composite elements (TESCAN MIRA 3, with SAMX Detector Czech Republic). The pH of zero point charge (pH_{ZPC}) was measured for determining the surface charge properties of the composite. The intermediate products of metronidazole degradation were detected by an Agilent Technologies 7890A gas chromatography (GC)/MS device. The biochar and composite surface area was

determined by the Brunauer–Emmett–Teller (BET) analysis (BELSORP MINI 2 Japan).

2.6. Process of test and analyses

The initial stock solution of metronidazole (1,000 mg L^{-1}) was prepared by dissolving the appropriate amount of the antibiotic powder in deionized distilled water. The one-factor-at-a-time method was used to optimize the variables affecting the efficiency of metronidazole removal; the parameters and their ranges were as follows: catalyst concentration (0.125, 0.25, 0.5, 0.75 and 1 g L^{-1}), pH (3, 5, 7, 9 and 11), initial metronidazole concentration (10, 15, 20, 30 and 40 mg L^{-1}), and contact time (5, 10, 15, 20, 30, 45, 60, 90 and 120 min). The present study also investigated the effect of radical trappers in the synthetic sample on metronidazole removal from urban drinking water and hospital wastewater, to which metronidazole was added. Each specimen was picked up after proper contact time and filtered using syringe filters with 0.25 µm pore size. The concentrations of metronidazole were determined by high-performance liquid chromatography (HPLC) (model Kanaure with UV-Vis detectors) at the wavelength of 319 nm. The column temperature, specimen injection rate, and flow rate were 35°C, 20 µl, and 1 mL min^{-1}, respectively. The mobile phase consisted of acetonitrile and distilled water solutions with HPLC grade of 30:70 ratios, respectively [45,46]. The remaining concentration of metronidazole in solutions was calculated using the area under a curve formula.

3. Results and discussion

3.1. Composite specifications

3.1.1. XRD analysis

The XRD patterns of the biochar, $Fe_3O_4/SiO_2/TiO_2$ nanocatalyst, and $Fe_3O_4/TiO_2/BC$ composite are shown in Fig. 1a. The main peaks of 2θ, 18.35°, 30.05°, 35.72°, 43.6°, 53.85°, 57.54°, 63.31° belong to the Fe_3O_4 nanoparticles; the TiO_2 peaks include 25.39°, 37.62°, 48°, 71.74° and 74.59°. The Biochar peak is 22° as shown in Fig. 1a. According to the XRD pattern, the refraction peaks in the $Fe_3O_4/TiO_2/BC$ composite are similar to the $Fe_3O_4/SiO_2/TiO_2$ nanocatalyst refraction peaks, except that in the composite there is an additional peak in the 22° region corresponding to the biochar. In addition, no additional refraction peak was observed in the XRD pattern of the $Fe_3O_4/TiO_2/BC$ composite, which confirms the purity of the material used in the catalyst synthesis [40,46].

3.1.2. FTIR analysis

The results of the FTIR analysis in the range of 450–4,000 cm^{-1} are presented in Fig. 1b. Specific absorption peaks shown in the figure had a distinctive absorption peak at 3,433.65 cm^{-1} belonging to the hydroxyl O–H group of the surface hydroxyl group. The absorption peak at 1,725.70 cm^{-1} indicates the presence of the carbonyl group. Also, the absorption peak at 1,632.29 cm^{-1} indicates the C=O bond [35]. Another distinct peak reflects the Si–O vibration, which is considered as the constituent element of the biochar. The absorption peak at 593.13 cm^{-1} is related to the Fe–O and

a)

b)

c)

d)

(Fig. 1. *Continued*)

e)

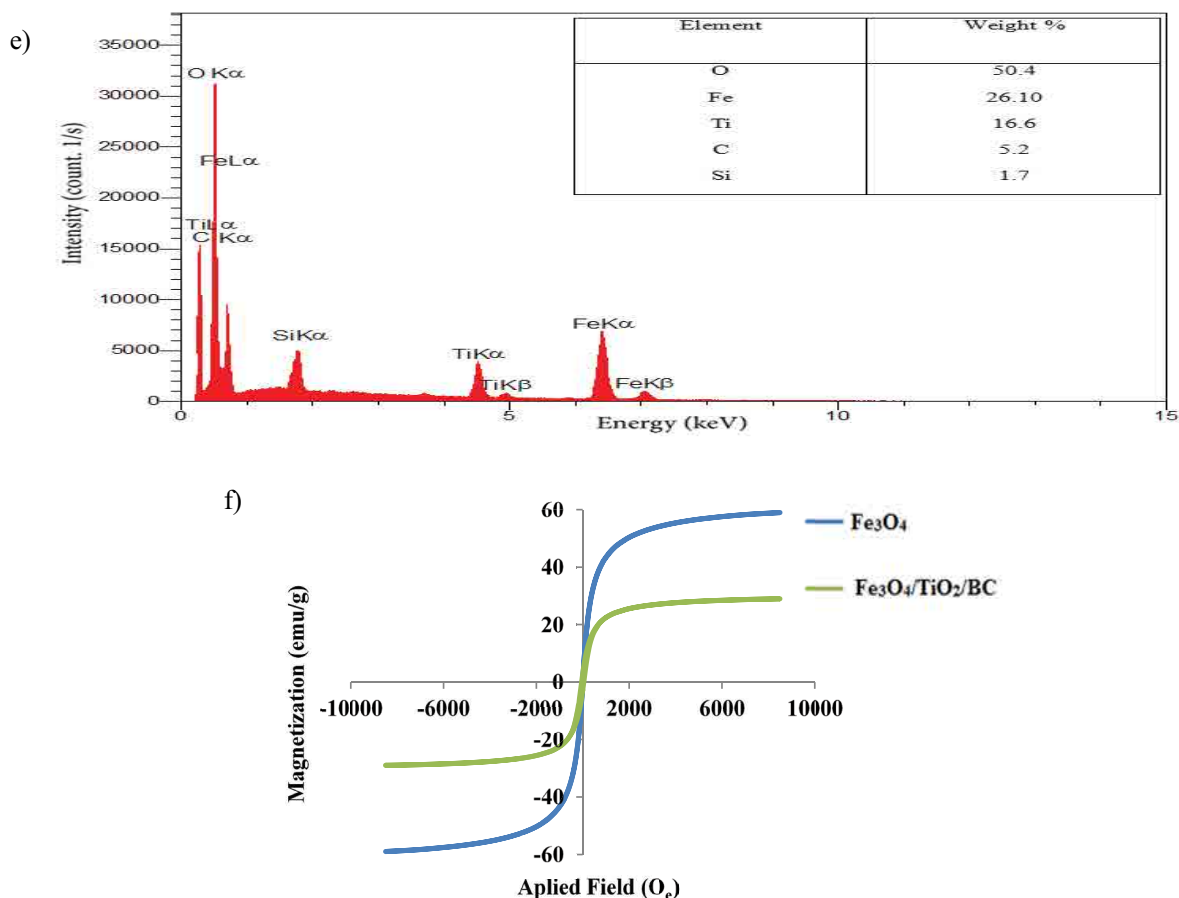| Element	Weight %
O	50.4
Fe	26.10
Ti	16.6
C	5.2
Si	1.7

f)
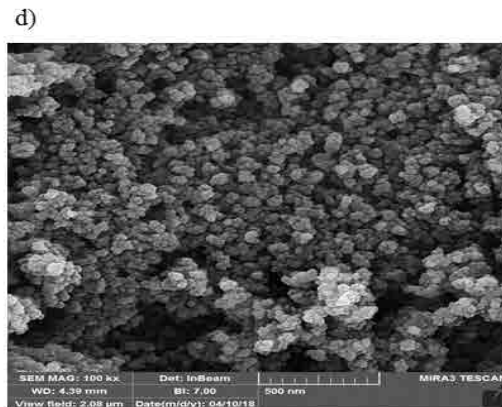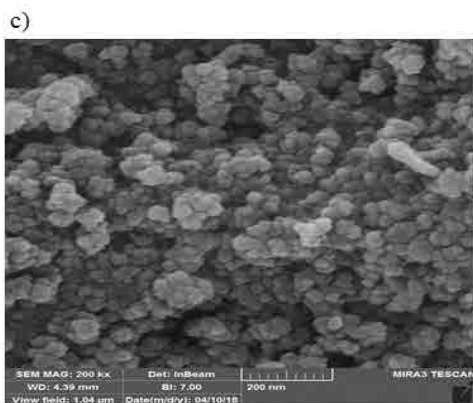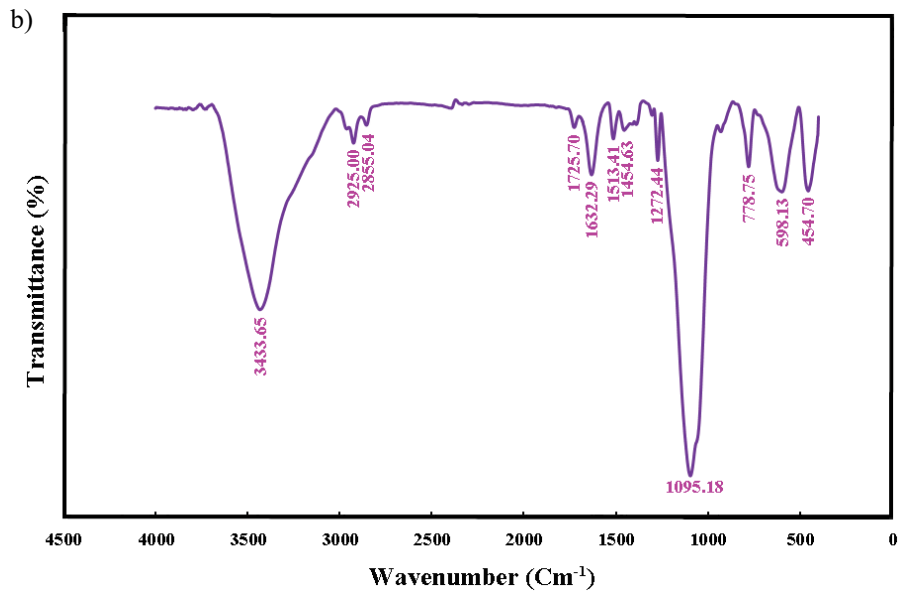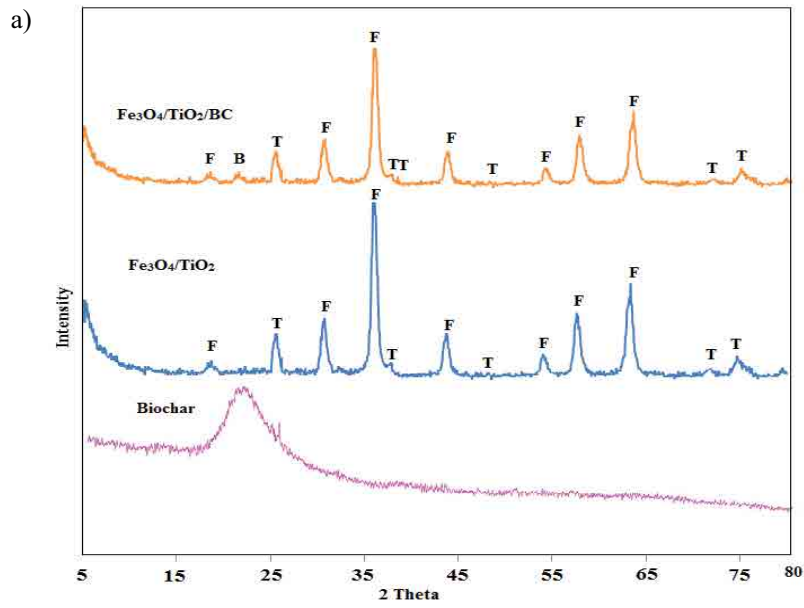
Fig. 1. Composite specifications (a) XRD analysis, (b) FTIR analysis, (c,d) SEM images and (e) EDX pattern and VSM analysis.

Ti–O–C vibration. Also, the absorption peak at 454.70 cm^{-1} is related to the Ti–o–Ti vibration [47].

3.1.3. SEM analysis

The morphology of the composite was investigated by SEM images (Figs. 1c and d). The average particle size was approximately 25 nm. The nanoparticles had a spherical structure; and, in the image TiO$_2$ is shown as the white layer illustrating its loading onto the composite. The surface of the hollow composite particles is fully flat and dense [43].

3.1.4. EDX analysis

EDX analysis was performed to identify the constituent elements of the composites. According to the results shown in Fig. 1e, the main constituent elements include oxygen, iron, titanium, and carbon, which indicate the successful development of the composite of Fe$_3$O$_4$, TiO$_2$, and carbon substrate.

3.1.5. Vibrating sample magnetometer analysis

Fig. 1f shows the vibrating sample magnetometer (VSM) diagrams of the composite and Fe$_3$O$_4$ at room temperature, for reconnoitring the magnetic properties of the sample. The magnetic saturation grade of Fe$_3$O$_4$ and the composite

are 58.97 and 28.97 emu g^{-1}, respectively. The reason for its decreased amount is probably related to the loading of TiO$_2$ on the surface of Fe$_3$O$_4$, as well as the reduction percentage of Fe$_3$O$_4$ in the composite sample compared to the pure Fe$_3$O$_4$. The synthesized sample shows good super paramagnetic behavior at room temperature. This feature helps the catalyst to be easily separated by being placed in an external magnetic field. Due to the magnetic properties of the composite, it is easy to separate it from the reaction medium by high magnetic characteristic and be reused considering the importance of recycling [48,49]. The degree of the composite's magnetic saturation decreased in comparison with Fe$_3$O$_4$ due to the presence of TiO$_2$ and biochar in the structure of the composite [50].

3.1.6. BET analysis

Table 2 shows the BET analysis results. The biochar-coated Fe$_3$O$_4$ and TiO$_2$ exhibited lower surface area as compared with that of biochar [43].

3.2. pH effect

Fig. 2 demonstrates the effect of pH on the composite-based metronidazole removal efficiency. As can be seen, the removal efficiency increased from 85% to 100% as pH

Table 2
BET analysis of Fe_3O_4, biochar and the composite

Sample	BET ($m^2 g^{-1}$)	Total pore volume ($p/p_0 = 0.990$)	D_p (nm)
Fe_3O_4	63.22	0.006	2.95
Biochar	460.96	0.2844	2.460
$Fe_3O_4/TiO_2/BC$	157.59	0.258	3.64

increased from 3 to 7. However, such efficiency decreased with further increase in pH value to 9 and 11. For example, the removal percentage declined to 85% at pH = 11. The composite pH_{zpc} was determined to be 7.5, with negative and positive composite surfaces, which were observed at pH values below and above 7.5. Also, in previous studies, it has been reported that the pH_{pzc} (isoelectric point) of a similar composite was in the range of 6–8 [26,30]. Therefore, more OH-ions are absorbed on the surface and radical hydroxyl production increases at pH values lower than pH_{zpc}. Since the pK_a of metronidazole is 2.55, it is thus present as a cation and anion at pH values of higher and lower than 2.55; therefore, the best metronidazole adsorption toward the composite occurs at pH values of lower than 7.5 at which the composite surface is positively charged and, at pH values higher than 2.55, metronidazole is present as an anion. The photocatalyst process is more efficient at neutral to-alkaline pHs than acidic pHs; this observation is consistent with the results of the related previous studies [51]. Moreover, the TiO_2 nanoparticles have an accumulation property in acidic conditions. As a result, it reduces the absorption of light and removal efficiency [52].

3.3. Effect of contact time and initial metronidazole concentration

Fig. 3 shows the effect of the initial concentration of metronidazole and contact time on the removal efficiency of the antibiotic from aqueous solution. As can be seen in the figure, with increasing the metronidazole concentration from 10 to 40 mg L^{-1}, the removal efficiency decreased from 100% to 80%; this is because of the fact that there are more metronidazole molecules in the aqueous solution that should be absorbed at the composite surface and removed in contact with the catalyst. By contrast, lower metronidazole concentration leads to an increase in the number of molecules having contact with the composite and, in turn, higher removal rate. However, when the concentration is raised, the removal efficiency decreases as, in this state, the composite content remains unchanged and metronidazole molecules tend less to be in contact with the composite [51]. Also, a greater amount of the pollutant causes the catalyst surface to be saturated. Also, active catalytic sites decrease, leading to a decline in removal efficiency [53]. By increasing the concentration of pollutants in water, it reduces the reactive species, disperses and decreases UV light penetration into the solution [53,54]. In photocatalytic processes, photocatalysts usually produce a pair of electrons-hole by photon absorption, which with a series of reactions hydroxyl radicals, which is a superoxide, are produced, that can react with the compounds. As a result, the reaction process will take
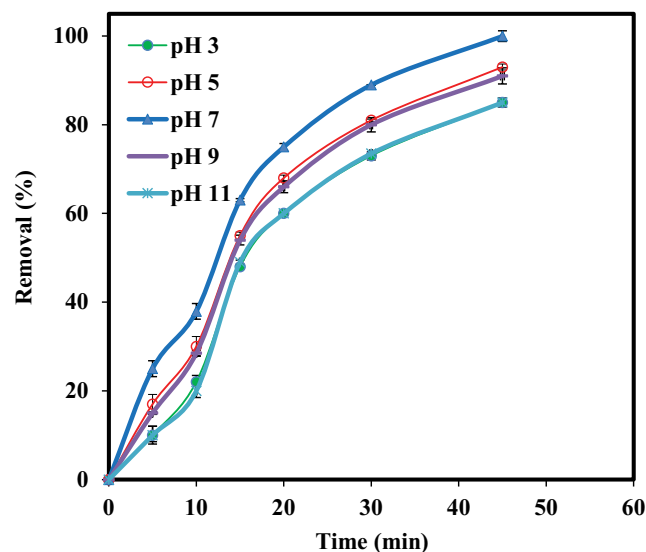

Fig. 2. Effect of solution pH on photocatalytic degradation of metronidazole (composite concentration = 0.35 g L^{-1}, metronidazole concentration = 20 mg L^{-1} and contact time = 90 min).
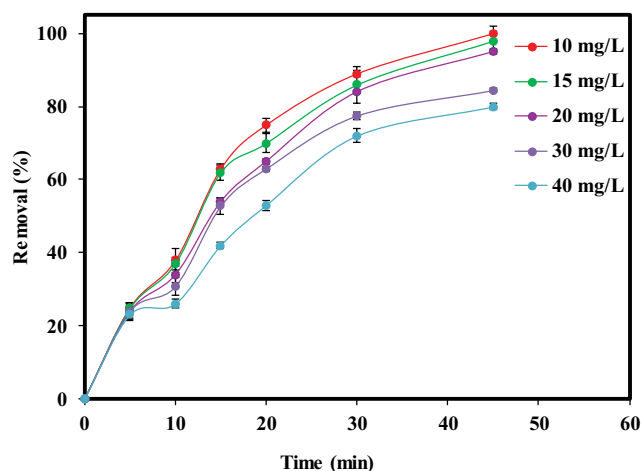

Fig. 3. Effect of contact time and initial metronidazole concentration on photocatalytic degradation (composite concentration = 0.35 g L^{-1} and pH = 7).

place at shorter contact times [55]. And, since the catalyst has been placed on the substrate stage and a composite is formed; thus, in the produced composite, the catalyst and pollutant have a larger surface area in comparison with the sole catalyst. This results in a decline in reaction time [35,56].

3.4. Effect of composite concentration

Fig. 4 shows the results obtained from changes in initial composite concentration on the photocatalytic removal efficiency of metronidazole. As can be seen, with increasing the initial concentration, the removal efficiency initially increased and then declined. An increase in composite concentration increased the removal efficiency, because it enhances both adsorption sites on the composite and production of radicals. The removal efficiency decreases
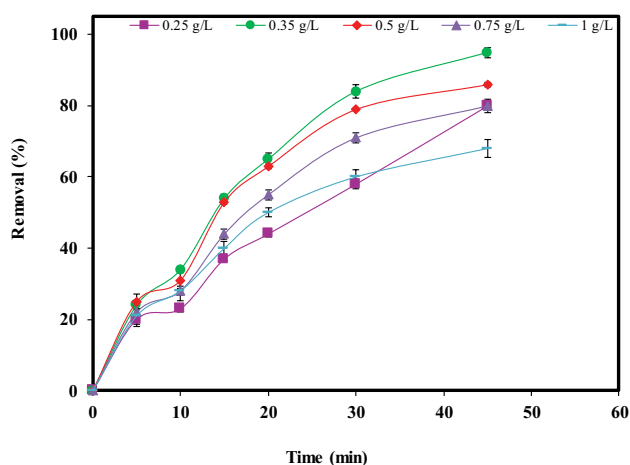
Fig. 4. Effect of composite concentration on photocatalytic degradation of metronidazole (metronidazole concentration = 10 mg L^{-1}, pH = 7, contact time = 45 min).

with increasing the composite concentration, which is due to a decrease in the intensity of the UV lamp blocked by increasing the composite concentration [57]. The results are consistent with those reported by other researchers [58,59].

3.5. Determination of the kinetic model

To obtain the kinetic model information, the Zero, first and second-order equations (by plotting $C_0 - C_t$, $\ln\dfrac{C_0}{C_t}$ and $\dfrac{1}{C_t} - \dfrac{1}{C_0}$ vs. time, respectively) were used [60–62]. Table 3 shows all equations and constant coefficients for various

metronidazole concentrations related to kinetic studies. The photocatalytic degradation of metronidazole followed a first-order kinetic model. The first-order rate constants of photocatalytic process (Kobs (min^{-1})) at different initial concentrations of metronidazole are shown in Table 4. Reaction rate (K_{obs}) of the first-order kinetic model decreased from 0.747 to 0.0367 m^{-1} with increasing metronidazole concentration from 10 to 40 mg L^{-1}. The K_{obs} value in various

Table 3
Kinetics models and parameters for metronidazole degradation [65–67]

Kinetic models	Parameters
Zero-order	C_0 (mg L^{-1}), C_t (mg L^{-1}),
$C_0 - C_t = k_0 t$	k_0 (mol/l min)
First-order	K_{obs} (min^{-1})
$\ln\dfrac{C_0}{C_t} = K_{obs} t$	
Second-order	K_2 (L mol^{-1} min^{-1})
$\dfrac{1}{C_t} - \dfrac{1}{C_0} = K_2 t$	

metronidazole concentrations was obtained by the diagram gradient of the $\ln\dfrac{[\text{metronidazole}]_0}{[\text{metronidazole}]_t}$ versus the reaction time [45,63]. With increasing the initial antibiotic concentration of, the reaction speed and regression degree decreased, which is consistent with the results of similar studies [26,58,64].

3.6. Comparison of important parameters effective in photocatalytic degradation of metronidazole between the present and other studies

In this section, the most important parameters affecting the photocatalytic removal of metronidazole surveyed in the present study and other similar studies have been compared. In this section, the most important parameters affecting the photocatalytic removal of metronidazole surveyed in the present study and other similar studies have been compared (Table 5).

3.7. Removal of metronidazole from urban drinking water and real hospital wastewater

In order to evaluate the efficiency of the Fe$_3$O$_4$/TiO$_2$/BC composite in real conditions, drinking water and real wastewater samples were examined. The metronidazole concentration was adjusted at 10 mg L^{-1}, which was found to be the optimal concentration, in all samples. The results are shown in Fig. 5. In this study, we evaluated the effect of the process on the metronidazole removal from drinking water containing a series of anions, cations, and other elements. Apparently, the removal efficiency decreased; this is mainly due to the presence of carbonate and bicarbonate ions which affect the radicals contributing to the degradation of pollutants. These ions may also deactivate the active sites on the composite surface effective in metronidazole removal. These findings are consistent with those of a related work [69]. Lower removal efficiency rate obtained for the wastewater sample is probably because of the presence of solids as well as the interference of ions like chloride, sulfate, Nitrate and phosphate or other organic contaminants. Besides, both organic and metronidazole molecules compete to react with reactive species. Also, high concentrations of organic matters reduce the efficiency of metronidazole removal [57,69]. Further, the formation of inorganic layers on the composite surface, which decreases the contact between the composite surface and the antibiotic, may be another reason for the declined efficiency rate [70].

3.8. Effect of radical scavenger

In the photocatalytic process, the surface of the catalyst under UV light causes the formation of charge carriers h$^+_{(VB)}$ and e$^-_{(CB)}$ and in the water the contaminants are absorbed onto the catalyst's surface [71]. In the presence of the oxygen molecule adjacent to the catalyst's surface, the electrons in the conduction band are trapped, and the oxygen molecule is reduced to radical superoxide [58,71]. In the next step, h$^+_{(VB)}$ (hole) reacts with the water molecule and produces radical hydroxyl and hydrogen ions [72]. In order to ensure radical production, in present study, we investigated the effect

Table 4
Kinetic parameters for the photocatalytic degradation of metronidazole at different concentrations of metronidazole ($Fe_3O_4/TiO_2/BC$ concentration = 0.35 g L^{-1} and pH = 7)

Metronidazole (mg L^{-1})	Zero-order		First-order			Second-order		
	k_0 (mol L^{-1} min^{-1})	R^2	K_{obs} (min^{-1})	$1/K_{obs}$ (min)	R^2	K_2 (L mol^{-1} min^{-1})	R^2	
10	0.218	0.87	0.0747	13.38	0.99	0.0288	0.86	
15	0.314	0.82	0.0689	14.51	0.99	0.0256	0.82	
20	0.4161	0.86	0.067	14.49	0.99	0.0198	0.80	
30	0.6119	0.88	0.0431	23.04	0.98	0.004	0.74	
40	0.698	0.84	0.0367	27.52	0.97	0.0023	0.89	

Table 5
Comparison of important parameters effective in photocatalytic degradation

System	pH	Catalyst concentration (g L^{-1})	[Metronidazole]$_0$ (mg L^{-1})	Lamp (W)	Time (min)	Removal efficiency (%)	Kinetic	K_{obs}	Reference
Fe^0/graphen-TiO_2	5	1	35	20	50	99.26	Pseudo-first-order	0.083	[59]
UV/TiO_2	7	0.5	40	125	120	99.48	Pseudo-first-order	0.00513	[45]
UV/TiO_2	6	1.5	10	100	60	86.10	Pseudo-first-order	0.045	[51]
UV/Zno	9.5	0.5	10	100	60	60.32	Pseudo-first-order	0.124	[51]
TiO_2-doped Fe^{3+}	11	0.5	80	125	120	97	Pseudo-first-order	0.027	[68]
UV/TiO_2	7	0.5	80	125	90	99.5	Pseudo-first-order		[32]
$Fe_3O_4/TiO_2/BC$	7	0.35	10	16	45	100	Pseudo-first-order	0.074	Present study

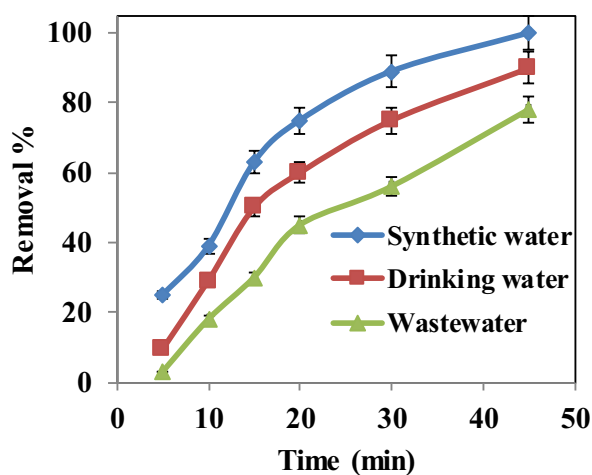
Fig. 5. Metronidazole removal from urban drinking water and real hospital wastewater under the optimum conditions.

Fig. 6. Effect of radical scavenger on photocatalytic degradation of metronidazole under the optimum conditions (metronidazole concentration = 10 mg L^{-1}, pH = 7, composite concentration = 0.35 g L^{-1}, contact time = 45 min).

of different types of radical scavengers on metronidazole removal efficiency under the fixed conditions as follows: metronidazole concentration of 10 mg L^{-1}, composite concentration of 0.35 g L^{-1}, and pH = 7 using benzoquinone, tert-butanol, and ammonium oxalate for superoxide ($O_2^{\bullet -}$), hydroxyl ($OH^\bullet$), and hole (h^+) trappers, respectively, at the optimal contact time. The results have been shown in Fig. 6. The removal efficiency in the presence of benzoquinone, tert-butanol, and ammonium oxalate decreased during the photocatalytic process as compared to absence of the these radical
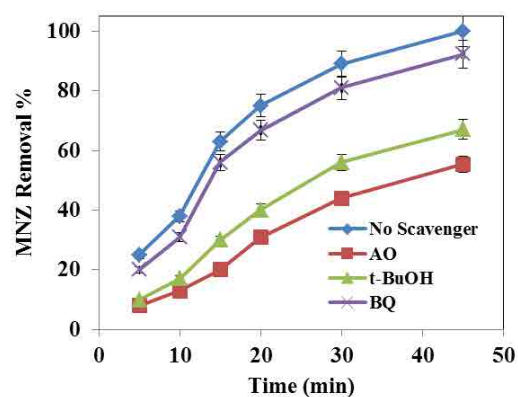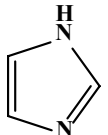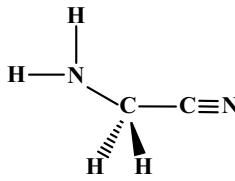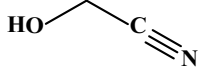
scavengers. In the case of absence of the radical scavengers, the removal efficiency was 100%, which decreased by 92.3%, 67.11% and 55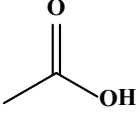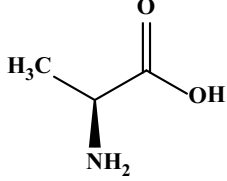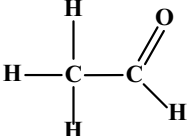.45% in the presence of benzoquinone, tert-butanol, and ammonium oxalate, respectively. The results of previous studies have illustrated that radical oxidation of contaminants is the most important removal mechanism in the photocatalytic oxidation. In general, the main reason for the photocatalytic mechanism for the composite-based metronidazole removal is hole (h^+), hydroxyl radical ($OH^\bullet$) and superoxide radical ($O_2^{-\bullet}$), respectively [51,73]. In the study by

Table 6
Characteristics and types of intermediate product of photocatalytic degradation of metronidazole

Molecular weight	Structure	Chemical formula	Composition name	Row
68.077		$C_3H_4N_2$	1H-Imidazole	1
56.07		$C_2H_4N_2$	Aminoacetonitrile	2
57.05		C_2H_3NO	Hydroxy acetonitrile	3
75.07		$C_2H_5NO_2$	Glycine	4
60.05		$C_2H_4O_2$	Acetic acids	5
89.09		$C_3H_7NO_2$	Alanine	6
44.05		C_2H_4O	Acetaldehyde	7
73.10		C_3H_7NO	Isoamyl benzyl ether	8

Tran et al. [51] on the removal of metronidazole by a TiO_2 nanocatalyst the presence of hole (h^+) was more effective than the other radical scavengers. In study by Wang et al. [59] where Fe_0/graphene-TiO_2 composite was used for photocatalytic removal of metronidazole from aqueous solution. The results showed that the greatest effect was observed after the addition of ammonium oxalate (h^+) and the second-order after the addition of methanol ($OH^•$).

3.9. Mineralization rate

The analysis of total organic carbon (TOC) contents through a TOC analyzer (Shimadzu VCHS/CSN, Japan) was performed to determine mineralization rates. Fig. 7 shows the mineralization percentages. Generally, the further contaminants are mineralized by the treatment process, the lower environmental hazards are caused by wastewater discharge. Therefore, it can be claimed that the process used in the current research can be applied for the degradation and mineralization of aquatic environments contaminated with metronidazole [59].

3.10. Intermediate products

After separation of the composite and under the optimal conditions, intermediate products were detected through a

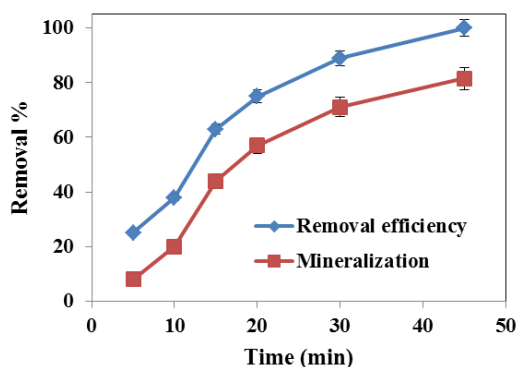Fig. 7. Mineralization rate of metronidazole during photocatalytic degradation under the optimum conditions (metronidazole concentration = 10 mg L^{-1}, pH = 7, composite concentration = 0.35 g L^{-1}, contact time = 45 min).

Fig. 8. Reuse exam for the photocatalytic degradation of metronidazole (composite concentration = 0.35 g L^{-1}, pH = 7, metronidazole = 10 mg L^{-1}, contact time = 45 min).

gas chromatography–mass spectroscopy (Agilent Technologies 7890A) device. First, the samples were prepared by the liquid–liquid extraction. Next, 2 ml of hexane was added to 5 ml of the sample in the test tube and mixed with vertex for 5 min. After being settled in the tube for 15 min, 10 µL of the solvent sample was removed and then injected into the GC device (7890A Agilent Technologies). Finally, the by-products were identified according to the device encyclopedia [51,69]. All by-products identified in this study are shown in Table 6. The photocatalytic reaction of metronidazole happens via the main oxidizing agents of holes (h$^+$) and radical hydroxyl. It takes place in two separate locations. The holes oxidizing agent (h$^+$) that directly attacks the hydroxyl group in metronidazole and converts to the carboxyl group. The whole reaction (h$^+$) is also applied to the group of branches, which is mentioned in another study [51]. The radical hydroxyl reaction causes the opening and destruction loops [74,75].

3.11. Reuse

Fig. 8 shows the effect of the recycling test on the efficiency of metronidazole removal. In this study, the efficiency was investigated in five cycles and the results showed that the high removal rates declined somewhat as moving from the first to the fifth cycle. Of course, the efficiency rate was 80% in the fifth cycle. Therefore, it can be reused to remove the metronidazole antibiotic. The decreased efficiency was probably caused by accumulation of organic intermediates in the hole and on the surface of the composite, which are effective in the adsorption of metronidazole [46].

4. Conclusions

The excessive consumption of antibiotics has led to their widespread presence in the environment; they find their ways to surface water, groundwater and drinking water. Antibiotics that are being used in the treatment of humans and animals are among the most important contaminants. In this study, the Fe$_3$O$_4$/TiO$_2$/BC composite, which was prepared with the sol-gel method, was used to provide a suitable solution for removing metronidazole antibiotic. The
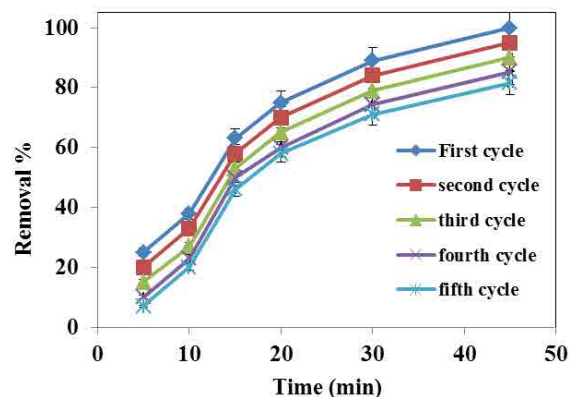
characterization of the composite illustrate that it had successfully been constructed. Maximum removal rate (100%) was obtained under the optimum conditions: pH = 7, composite concentration 0.35 g L^{-1} and contact time 45 min. In order to affect the intervention, the examination was done in the presence of the scavenger, by using drinking water and real hospital wastewater. The results showed the removal efficiency decreased in the presence of interveners. The removal efficiency of metronidazole was investigated in five cycles and the results indicated the high efficiency was somewhat reduced as moving from the first to the fifth cycle; the efficiency rate was 80% in the fifth cycle.

References

[1] T. Pirom, T. Wongsawa, T. Wannachod, N. Sunsandee, U. Pancharoen, S. Kheawhom, Amoxicillin removal from aqueous solutions using hollow fibre supported liquid membrane: kinetic study, Chem. Pap., 71 (2017) 1291–1302.

[2] M.H. Dehghani, A. Zarei, M. Yousefi, Efficiency of ultrasound for degradation of an anionic surfactant from water: surfactant determination using methylene blue active substances method, MethodsX, 6 (2019) 805–814.

[3] N. Jafarzadeh, H. Rezazadeh, Z. Ramezani, S. Jorfi, M. Ahmadi, H. Ghariby, G. Barzegar, Taguchi optimization approach for metronidazole removal from aqueous solutions by using graphene oxide functionalized β-cyclodextrin/Ag nanocomposite, Water Sci. Technol., (2017) 36–47, doi: 10.2166/wst.2018.080.

[4] S.A. Mousavi, H. Janjani, Antibiotics adsorption from aqueous solutions using carbon nanotubes: a systematic review, Toxin Rev., (2018) 1–12, https://doi.org/10.1080/15569543.2018.1483405.

[5] L. Sun, D.M. Chen, S.G. Wan, Z.B. Yu, Adsorption studies of dimetridazole and metronidazole onto biochar derived from sugarcane bagasse: kinetic, equilibrium, and mechanisms, J. Polym. Environ., 26 (2018) 765–777.

[6] A. Dehghan, A. Zarei, J. Jaafari, M. Shams, A.M. Khaneghah, Tetracycline removal from aqueous solutions using zeolitic imidazolate frameworks with different morphologies: a mathematical modeling, Chemosphere, 217 (2019) 250–260.

[7] A. Yeh, D.J. Marcinek, J.P. Meador, E.P. Gallagher, Effect of contaminants of emerging concern on liver mitochondrial function in Chinook salmon, Aquat. Toxicol., 190 (2017) 21–31.

[8] J.L. Acero, F.J. Benitez, F.J. Real, F. Teva, Removal of emerging contaminants from secondary effluents by micellar-enhanced ultrafiltration, Sep. Purif. Technol., 181 (2017) 123–131.

[9] R. Khosravi, A. Zarei, M. Heidari, A. Ahmadfazeli, M. Vosughi, M. Fazlzadeh, Application of ZnO and TiO$_2$ nanoparticles coated onto montmorillonite in the presence of H$_2$O$_2$ for efficient removal of cephalexin from aqueous solutions, Korean J. Chem. Eng., 35 (2018) 1000–1008.

[10] B. Petrie, R. Barden, B. Kasprzyk-Hordern, A review on emerging contaminants in wastewaters and the environment: current knowledge, understudied areas and recommendations for future monitoring, Water Res., 72 (2015) 3–27.

[11] A.M. Gorito, A.R. Ribeiro, C.M.R. Almeida, A.M.T. Silva, A review on the application of constructed wetlands for the removal of priority substances and contaminants of emerging concern listed in recently launched EU legislation, Environ. Pollut., 227 (2017) 428–443.

[12] R. Loos, R. Carvalho, D.C. António, S. Comero, G. Locoro, S. Tavazzi, B. Paracchini, M. Ghiani, T. Lettieri, L. Blaha, B. Jarosova, S. Voorspoels, K. Servaes, P. Haglund, J. Fick, R.H. Lindberg, D. Schwesig, B.M. Gawlik, EU-wide monitoring survey on emerging polar organic contaminants in wastewater treatment plant effluents, Water Res., 47 (2013) 6475–6487.

[13] T.S. Oliveira, M. Murphy, N. Mendola, V. Wong, D. Carlson, L. Waring, Characterization of pharmaceuticals and personal care products in hospital effluent and waste water influent/effluent by direct-injection LC-MS-MS, Sci. Total Environ., 518 (2015) 459–478.

[14] E. Brillas, I. Sirés, Electrochemical removal of pharmaceuticals from water streams: reactivity elucidation by mass spectrometry, TrAC, Trends Anal. Chem., 70 (2015) 112–121.

[15] K.M. Hansen, A. Spiliotopoulou, R.K. Chhetri, M.E. Casas, K. Bester, H.R. Andersen, Ozonation for source treatment of pharmaceuticals in hospital wastewater – ozone lifetime and required ozone dose, Chem. Eng. J., 290 (2016) 507–514.

[16] B. Kakavandi, A. Takdastan, N. Jaafarzadeh, M. Azizi, A. Mirzaei, A. Azari, Application of Fe$_3$O$_4$@C catalyzing heterogeneous UV-Fenton system for tetracycline removal with a focus on optimization by a response surface method, J. Photochem. Photobiol., A, 314 (2016) 178–188.

[17] B. Kakavandi, A. Esrafili, A. Mohseni-Bandpi, A. Jonidi Jafari, R. Rezaei Kalantary, Magnetic Fe$_3$O$_4$@C nanoparticles as adsorbents for removal of amoxicillin from aqueous solution, Water Sci. Technol., 69 (2014) 147–155.

[18] A. Habibi, L.S. Belaroui, A. Bengueddach, A.L. Galindo, C.I.S. Díaz, A. Peña, Adsorption of metronidazole and spiramycin by an Algerian palygorskite. Effect of modification with tin, Microporous Mesoporous Mater., 268 (2018) 293–302.

[19] J.S. Jeong, W.H. Song, W.J. Cooper, J.Y. Jung, J. Greaves, Degradation of tetracycline antibiotics: mechanisms and kinetic studies for advanced oxidation/reduction processes, Chemosphere, 78 (2010) 533–540.

[20] J.-Y. Cho, Evaluation of degradation of antibiotic tetracycline in pig manure by electron beam irradiation, Bull. Environ. Contam. Toxicol., 84 (2010) 450–453.

[21] J.W. Peterson, L.J. Petrasky, M.D. Seymour, R.S. Burkhart, A.B. Schuiling, Adsorption and breakdown of penicillin antibiotic in the presence of titanium oxide nanoparticles in water, Chemosphere, 87 (2012) 911–917.

[22] Q.M. Xian, L.X. Hu, H.C. Chen, Z.Z. Chang, H.X. Zou, Removal of nutrients and veterinary antibiotics from swine wastewater by a constructed macrophyte floating bed system, J. Environ. Manage., 91 (2010) 2657–2661.

[23] A.M. Deegan, B. Shaik, K. Nolan, K. Urell, M. Oelgemöller, J. Tobin, A. Morrissey, Treatment options for wastewater effluents from pharmaceutical companies, Int. J. Environ. Sci. Technol., 8 (2011) 649–666.

[24] K.L. Jury, T. Vancov, R.M. Stuetz, S.J. Khan, Antibiotic resistance dissemination and sewage treatment plants, Curr. Res. Technol. Educ. Top. Appl. Microbiol. Microbial Biotechnol., 2 (2010) 509–510.

[25] M.B. Ahmed, J.L. Zhou, H.H. Ngo, W.S. Guo, Adsorptive removal of antibiotics from water and wastewater: progress and challenges, Sci. Total Environ., 532 (2015) 112–126.

[26] M. Ahmadi, H.R. Motlagh, N. Jaafarzadeh, A. Mostoufi, R. Saeedi, G. Barzegar, S. Jorfi, Enhanced photocatalytic degradation of tetracycline and real pharmaceutical wastewater using MWCNT/TiO$_2$ nano-composite, J. Environ. Manage., 186 (2017) 55–63.

[27] W.A. Khanday, B.H. Hameed, Zeolite-hydroxyapatite-activated oil palm ash composite for antibiotic tetracycline adsorption, Fuel, 215 (2018) 499–505.

[28] J. Tong, X.T. Lu, J.Y. Zhang, I. Angelidaki, Y.S. Wei, Factors influencing the fate of antibiotic resistance genes during thermochemical pretreatment and anaerobic digestion of pharmaceutical waste sludge, Environ. Pollut., 243 (2018) 1403–1413.

[29] J. Zhang, Q. Sui, J. Tong, H. Zhong, Y. Wang, M. Chen, Y. Wei, Soil types influence the fate of antibiotic-resistant bacteria and antibiotic resistance genes following the land application of sludge composts, Environ. Int., 118 (2018) 34–43.

[30] D.E. Santiago, L.M. Pastrana-Martínez, E. Pulido-Melián, J. Araña, J.L. Faria, A.M.T. Silva, Ó. González-Díaz, J.M. Doña-Rodríguez, TiO$_2$-based (Fe$_3$O$_4$, SiO$_2$, reduced graphene oxide) magnetically recoverable photocatalysts for imazalil degradation in a synthetic wastewater, Environ. Sci. Pollut. Res., 25 (2018) 27724–27736.

[31] Y. Wu, E. Cui, Y. Zuo, W. Cheng, H. Chen, Fate of antibiotic and metal resistance genes during two-phase anaerobic digestion of residue sludge revealed by metagenomic approach, Environ. Sci. Pollut. Res., 25 (2018) 13956–13963.

[32] N. Okhovat, M. Hashemi, A.A. Golpayegani, Photocatalytic decomposition of Metronidazolein aqueous solutions using titanium dioxide nanoparticles, J. Mater. Environ. Sci., 6 (2015) 792–799.

[33] A. Aboudalle, H. Djelal, F. Fourcade, L. Domergue, A.A. Assadi, T. Lendormi, S. Taha, A. Amrane, Metronidazole removal by means of a combined system coupling an electro-Fenton process and a conventional biological treatment: by-products monitoring and performance enhancement, J. Mater. Environ. Sci., 359 (2018) 85–95.

[34] S. Miralles-Cuevas, F. Audino, I. Oller, R. Sánchez-Moreno, J.A. Sánchez Pérez, S. Malato, Pharmaceuticals removal from natural water by nanofiltration combined with advanced tertiary treatments (solar photo-Fenton, photo-Fenton-like Fe(III)–EDDS complex and ozonation), Sep. Purif. Technol., 122 (2014) 515–522.

[35] S. Banerjee, P. Benjwal, M. Singh, K.K. Kar, Graphene oxide (rGO)-metal oxide (TiO$_2$/Fe$_3$O$_4$) based nanocomposites for the removal of methylene blue, Appl. Surf. Sci., 439 (2018) 560–568.

[36] S. Pakdaman, A.E. Pirbazari, N. Gilani, Deposition of Ag nanoparticles onto TiO$_2$/Fe$_3$O$_4$/MWCNTs quaternary nano-composite: a visible-light-driven plasmonic photocatalyst for degradation of 2,4-dichlorophenol, Desal. Wat. Treat., 102 (2018) 241–252.

[37] M.S. Siboni, M.R. Samarghandi, J.-K. Yang, S.-M. Lee, Photo-catalytic removal of cyanide with illuminated TiO$_2$, Water Sci. Technol., 64 (2011) 1383–1387.

[38] Y.H. Ao, J.J. Xu, X.W. Shen, D.G. Fu, C.W. Yuan, Magnetically separable composite photocatalyst with enhanced photo-catalytic activity, J. Hazard. Mater., 160 (2008) 295–300.

[39] M. Gholami, M. Shirzad-Siboni, M. Farzadkia, J.-K. Yang, Synthesis, characterization, and application of ZnO/TiO$_2$ nanocomposite for photocatalysis of a herbicide (Bentazon), Desal. Wat. Treat., 57 (2016) 13632–13644.

[40] X.H. Jia, R.R. Dai, D.D. Lian, S. Han, X.Y. Wu, H.J. Song, Facile synthesis and enhanced magnetic, photocatalytic properties of one-dimensional Ag@Fe$_3$O$_4$-TiO$_2$, Appl. Surf. Sci., 392 (2017) 268–276.

[41] M. Shirzad-Siboni, A. Khataee, B. Vahid, S.W. Joo, Synthesis, characterization and immobilization of ZnO nanosheets on scallop shell for photocatalytic degradation of an insecticide, Sci. Adv. Mater., 7 (2015) 806–814.

[42] A. Gholizadeh, M. Kermani, M. Gholami, M. Farzadkia, Kinetic and isotherm studies of adsorption and biosorption processes in the removal of phenolic compounds from aqueous solutions: comparative study, J. Environ. Health Sci. Eng., 11 (2013) 29.

[43] S. Jorfi, B. Kakavandi, H.R. Motlagh, M. Ahmadi, N. Jaafarzadeh, A novel combination of oxidative degradation for

benzotriazole removal using TiO_2 loaded on $Fe^{II}Fe_2^{III}O_4$@C as an efficient activator of peroxymonosulfate, Appl. Catal., B, 219 (2017) 216–230.

[44] H.F. Zhou, C. Zhang, X.D. Wang, H.Q. Li, Z.J. Du, Fabrication of TiO_2-coated magnetic nanoparticles on functionalized multi-walled carbon nanotubes and their photocatalytic activity, Synth. Met., 161 (2011) 2199–2205.

[45] M. Farzadkia, E. Bazrafshan, A. Esrafili, J.-K. Yang, M. Shirzad-Siboni, Photocatalytic degradation of Metronidazole with illuminated TiO_2 nanoparticles, J. Environ. Health Sci. Eng., 13 (2015) 35.

[46] Y.Y. Luo, Z.Y. Lu, Y.H. Jiang, D.D. Wang, L.L. Yang, P.W. Huo, Z.L. Da, X.L. Bai, X.L. Xie, P.Y. Yang, Selective photodegradation of 1-methylimidazole-2-thiol by the magnetic and dual conductive imprinted photocatalysts based on TiO_2/Fe_3O_4/MWCNTs, Chem. Eng. J., 240 (2014) 244–252.

[47] Q.H. He, Z.X. Zhang, J.W. Xiong, Y.Y. Xiong, H. Xiao, A novel biomaterial — Fe_3O_4:TiO_2 core-shell nano particle with magnetic performance and high visible light photocatalytic activity, Opt. Mater., 31 (2008) 380–384.

[48] T.C. Cheng, K.S. Yao, N. Yeh, C.I. Chang, H.C. Hsu, Y.T. Chien, C.Y. Chang, Visible light activated bactericidal effect of TiO_2/Fe_3O_4 magnetic particles on fish pathogens, Surf. Coat. Technol., 204 (2009) 1141–1144.

[49] N. Esmaeili, A.E. Pirbazari, Z. Khodaee, Visible-light active and magnetically recyclable Ag-coated Fe_3O_4/TiO_2 nanocomposites for efficient photocatalytic oxidation of 2,4-dichlorophenol, Desal. Wat. Treat., 114 (2018) 251–264.

[50] F. Shi, Y.G. Li, Q.H. Zhang, H.Z. Wang, Synthesis of Fe_3O_4/C/TiO_2 magnetic photocatalyst via vapor phase hydrolysis, Int. J. Photoenergy, 2012 (2012) 8 p.

[51] M.L. Tran, C.-C. Fu, R.-S. Juang, Removal of metronidazole by TiO_2 and ZnO photocatalysis: a comprehensive comparison of process optimization and transformation products, Environ. Sci. Pollut. Res., 25 (2018) 28285–28295.

[52] X.-D. Zhu, Y.-J. Wang, R.-J. Sun, D.-M. Zhou, Photocatalytic degradation of tetracycline in aqueous solution by nanosized TiO_2, Chemosphere, 92 (2013) 925–932.

[53] L. Zhang, X.Y. Song, X.Y. Liu, L.J. Yang, F. Pan, J. Lv, Studies on the removal of tetracycline by multi-walled carbon nanotubes, Chem. Eng. J., 178 (2011) 26–33.

[54] M.E. Balmer, H.-R. Buser, M.D. Müller, T. Poiger, Occurrence of some organic UV filters in wastewater, in surface waters, and in fish from Swiss lakes, Environ. Sci. Technol., 39 (2005) 953–962.

[55] T. Cordero, J.-M. Chovelon, C. Duchamp, C. Ferronato, J. Matos, Surface nano-aggregation and photocatalytic activity of TiO_2 on H-type activated carbons, Appl. Catal., B, 73 (2007) 227–235.

[56] L.P. Ren, W. Zhou, B.J. Sun, H.Z. Li, P.H. Qiao, Y.C. Xu, J.X. Wu, K. Lin, H.G. Fu, Defects-engineering of magnetic γ-Fe_2O_3 ultrathin nanosheets/mesoporous black TiO_2 hollow sphere heterojunctions for efficient charge separation and the solar-driven photocatalytic mechanism of tetracycline degradation, Appl. Catal., B, 240 (2019) 319–328.

[57] J.K. Yang, S.M. Lee, M.S. Siboni, Effect of different types of organic compounds on the photocatalytic reduction of Cr(VI), Environ. Technol., 33 (2012) 2027–2032.

[58] E.O. Oseghe, A.E. Ofomaja, Study on light emission diode/carbon modified TiO_2 system for tetracycline hydrochloride degradation, J. Photochem. Photobiol., A, 360 (2018) 242–248.

[59] X.Y. Wang, A. Wang, M.Y. Lu, J. Ma, Synthesis of magnetically recoverable Fe^0/graphene-TiO_2 nanowires composite for both reduction and photocatalytic oxidation of metronidazole, Chem. Eng. J., 337 (2018) 372–384.

[60] A.A. Mohammadi, A. Zarei, H. Alidadi, M. Afsharnia, M. Shams, Two-dimensional zeolitic imidazolate framework-8 for efficient removal of phosphate from water, process modeling, optimization, kinetic, and isotherm studies, Desal. Wat. Treat., 129 (2018) 244–254.

[61] M.H. Dehghani, S. Kamalian, M. Shayeghi, M. Yousefi, Z. Heidarinejad, S. Agarwal, V.K. Gupta, High-performance removal of diazinon pesticide from water using multi-walled carbon nanotubes, Microchem. J., 145 (2019) 486–491.

[62] H.N. Saleh, M.H. Dehghani, R. Nabizadeh, A.H. Mahvi, K. Yaghmaeian, F. Hossein, M. Ghaderpoori, M. Yousefi, A. Mohammadi, Data on the acid black 1 dye adsorbtion from aqueous solutions by low-cost adsorbent-Cerastoderma lamarcki shell collected from the northern coast of Caspian Sea, Data Brief, 17 (2018) 774–780.

[63] M. Farzadkia, A. Esrafili, M.A. Baghapour, Y.D. Shahamat, N. Okhovat, Degradation of metronidazole in aqueous solution by nano-ZnO/UV photocatalytic process, Desal. Wat. Treat., 52 (2014) 4947–4952.

[64] W. Guissouma, O. Hakami, A.J. Al-Rajab, J. Tarhouni, Risk assessment of fluoride exposure in drinking water of Tunisia, Chemosphere, 177 (2017) 102–108.

[65] M. Yousefi, R. Nabizadeh, M. Alimohammadi, A.A. Mohammadi, A.H. Mahvi, Removal of phosphate from aqueous solutions using granular ferric hydroxide process optimization by response surface methodology, Desal. Wat. Treat., 158 (2019) 290–300.

[66] S. Mazloomi, M. Yousefi, H. Nourmoradi, M. Shams, Evaluation of phosphate removal from aqueous solution using metal organic framework; isotherm, kinetic and thermodynamic study, J. Environ. Health Sci. Eng., 17 (2019) 209–218.

[67] S. Ayub, A.A. Mohammadi, M. Yousefi, F. Changani, Performance evaluation of agro-based adsorbents for the removal of cadmium from wastewater, Desal. Wat. Treat., 142 (2019) 293–299.

[68] M. Malakootian, N. Olama, M. Malakootian, A. Nasiri, Photocatalytic degradation of metronidazole from aquatic solution by TiO_2-doped Fe^{3+} nano-photocatalyst, Int. J. Environ. Sci. Technol., 16 (2019) 4275–4284.

[69] Y.C. Deng, L. Tang, G.M. Zeng, J.J. Wang, Y.Y. Zhou, J.J. Wang, J. Tang, L.L. Wang, C.Y. Feng, Facile fabrication of mediator-free Z-scheme photocatalyst of phosphorous-doped ultrathin graphitic carbon nitride nanosheets and bismuth vanadate composites with enhanced tetracycline degradation under visible light, J. Colloid Interface Sci., 509 (2018) 219–234.

[70] M.L. Tran, C.-C. Fu, R.-S. Juang, Effects of water matrix components on degradation efficiency and pathways of antibiotic metronidazole by UV/TiO_2 photocatalysis, J. Mol. Liq., 276 (2019) 32–38.

[71] K. Ikehata, N. Jodeiri Naghashkar, M. Gamal El-Din, Degradation of aqueous pharmaceuticals by ozonation and advanced oxidation processes: a review, Ozone Sci. Eng., 28 (2006) 353–414.

[72] M.H. Cao, P.F. Wang, Y.H. Ao, C. Wang, J. Hou, J. Qian, Visible light activated photocatalytic degradation of tetracycline by a magnetically separable composite photocatalyst: graphene oxide/magnetite/cerium-doped titania, J. Colloid Interface Sci., 467 (2016) 129–139.

[73] S. Feizpoor, A. Habibi-Yangjeh, Ternary TiO_2/Fe_3O_4/$CoWO_4$ nanocomposites: novel magnetic visible-light-driven photocatalysts with substantially enhanced activity through p-n heterojunction, J. Colloid Interface Sci., 524 (2018) 325–336.

[74] H.B. Ammar, M.B. Brahim, R. Abdelhédi, Y. Samet, Green electrochemical process for metronidazole degradation at BDD anode in aqueous solutions via direct and indirect oxidation, Sep. Purif. Technol., 157 (2016) 9–16.

[75] L. Tong, S. Pérez, C. Gonçalves, F. Alpendurada, Y. Wang, D. Barceló, Kinetic and mechanistic studies of the photolysis of metronidazole in simulated aqueous environmental matrices using a mass spectrometric approach, Anal. Bioanal. Chem., 399 (2011) 421–428.